Relativistic coupled-cluster calculations on hyperfine structures and electromagnetic transition amplitudes of In III

Sourav Roy, Narendra Nath Dutta, and Sonjoy Majumder

Department of Physics, Indian Institute of Technology Kharagpur, Kharagpur, West Bengal 721302, India

Hyperfine constants and anomalies of ground as well as a few low-lying excited states of ^{113,115,117}In III are studied with highly correlated relativistic coupled-cluster theory. The ground-state hyperfine splitting of ^{115}In III is estimated to be 106.8 GHz. A shift of almost 1.9 GHz of the above frequency has been calculated due to the modified nuclear dipole moment. This splitting result shows its applicability as communication band and frequency standards at 10^{-11} s. A correlation study of hyperfine constants indicates a few distinct features of many-body effects in the wave functions in and near the nuclear region of this ion. Astrophysically important forbidden transition amplitudes are estimated. The calculated oscillator strengths of a few allowed transitions are compared with recent experimental and theoretical results wherever available.

I. INTRODUCTION

Recent trapping of doubly ionized Yb [1] can enhance the possibility of the trapping of doubly ionized In using the same experimental mechanism. Trapped ^{113}Cd II is known as an ideal candidate for the frequency standard and quantum computing [2,3]. Being in the same Ag isoelectronic sequence, ^{113,115,117}In III is also interesting due to its expected large hyperfine splitting like ^{113}Cd$^+$, as it is next to the latter ion in this sequence, has a nuclear g factor close to that of ^{113}Cd, and has a large nuclear spin ($I = 4.5$ for all these In isotopes, but $I = 1.5$ for ^{113}Cd). The discrepancies between experimental [4–6] and theoretical [7,8] estimations of magnetic dipole hyperfine constants of ^{115}In I indicate the possibility of a small variation of the nuclear moment obtained from Raghavan [9]. This is, however, very important for nuclear theory and physics where precise nuclear parameters are important, such as parity nonconservation (PNC) estimations [10–12]. The study of nuclear magnetization distribution on the indium isotopes has been an interesting topic in terms of its puzzling giant hyperfine anomaly [13–15]. The magnetic property can be estimated from their hyperfine anomalies (the Bohr-Weisskopf effect only [16,17]). These are calculated using accurate estimations of the hyperfine splitting of states. Study of this anomaly over different levels of atomic ionizations provides the ionization effect on the nucleus. The results obtained should provide a useful calibration for nuclear theory as well as reduce limitations of precise measurement of fundamental constants, such as parity and/or time violation constants, due to the uncertainty of neutron distribution [12,18].

Strong resonance lines from In III are required in order to provide the most important data for abundance analysis in various astronomical systems as well as laboratory plasmas [19–22]. Explanation of the observed large discrepancies between experimental [19,23] and theoretical [20] line broadening results in the optical spectrum [23] of In III requires precise estimations of allowed transitions. Whereas, the forbidden transitions are the effective decay mechanism in low-density hot plasmas where the possibility of collisional deexcitation is low [24]. Over the years there have been many experimental and theoretical endeavors to estimate the strengths of some ultraviolet or visible lines of this ion [25–32]. However, due to the large discrepancies among the results, correlation-exhaustive relativistic *ab initio* calculations are required. Also, we augment the database with lifetime of few other low-lying states.

Here we employ a highly correlated relativistic coupled-cluster (RCC) method based on the Dirac-Coulomb-Gaunt Hamiltonian to generate the ground and different excited states [33] of In III. With respect to other well known theories, the coupled-cluster theory has the potential to investigate electron correlation in an exhaustive way [3,34]. The various kinds of many-body effects such as core correlation, core polarization, and pair correlation are studied in the framework of the present RCC theory using the calculations of the hyperfine constants.

II. THEORY

In order to obtain a correlated wave function $|\Psi_v\rangle$ corresponding to a single-valence atomic state having a valence electron in the vth orbital, we solve the corresponding energy eigenvalue equation where the Dirac-Coulomb-Gaunt Hamiltonian is considered [33]. In the coupled-cluster theory, one can write this correlated wave function as [3,34–36]

$$|\Psi_v\rangle = e^T \{1 + S_v\}|\Phi_v\rangle, \tag{2.1}$$

where $|\Phi_v\rangle$ is the Dirac-Fock reference-state wave function that is generated in the V^{N-1} potential following Koopman's theorem [37], T is the closed-shell cluster operator that takes all the single and double excitations from the core orbitals [34], and S_v is the open-shell cluster operator that behaves like T but excites at least one electron from the valence v [34]. In the present approach, nonlinear coupled-cluster theory is used with the inclusion of partial triple excitations to solve the closed- and open-shell cluster amplitudes. This formalism is discussed in detail in Ref. [38].

The general matrix element of an operator $\hat{O}$ can be conveniently expressed with normalization as

$$O_{fi} = \frac{\langle \Psi_f | \hat{O} | \Psi_i \rangle}{\sqrt{\langle \Psi_f | \Psi_f \rangle \langle \Psi_i | \Psi_i \rangle}} = \frac{\langle \Phi_f | \{1 + S_f^\dagger\} e^{T^\dagger} \hat{O} e^T \{1 + S_i\} | \Phi_i \rangle}{\sqrt{\langle \Phi_f | \{1 + S_f^\dagger\} e^{T^\dagger} e^T \{1 + S_f\} | \Phi_f \rangle \langle \Phi_i | \{1 + S_i^\dagger\} e^{T^\dagger} e^T \{1 + S_i\} | \Phi_i \rangle}}$$

$$= \frac{\langle \Phi_f | \{1 + S_f^\dagger\} \overline{O} \{1 + S_i\} | \Phi_i \rangle}{N} = \frac{\langle \Phi_f | (\overline{O} + S_f^\dagger \overline{O} + \overline{O} S_i + S_f^\dagger \overline{O} S_i) | \Phi_i \rangle}{N}. \tag{2.2}$$

Here N is the normalization correction, and $\bar{O} = e^{\dagger T} \hat{O} e^T$ is a nontruncated series. However, the series is truncated in considering effective one-body and two-body operators in the present calculations. These effective operators arise from the contractions and noncontractions among the operators $\hat{O}$, $T^\dagger$, and T. These effective operators are then contracted with the S and $S^\dagger$ operators to evaluate the final matrix elements as represented by Eq. (2.2). Effective three-body operators can also arise, but are tedious to handle. Higher-body effective operators cannot be contracted with the S and $S^\dagger$ operators to calculate the matrix element. A coupled-cluster scheme that uses property calculations without truncation is given in detail by Mani and Angom [39] and theoretically can be a little more accurate with respect to the truncation we consider here.

The contractions of the effective one-body terms with the S and $S^\dagger$ operators provide the most important contributions to the matrix elements [3]. The term $\overline{O}$ represents the sum of the Dirac-Fock (DF) and the core-correlation contribution. The lowest-order pair-correlation and core-polarization effects arise from the terms $\overline{O}S_1 + S_1^\dagger \overline{O}$ and $\overline{O}S_2 + S_2^\dagger \overline{O}$, respectively. In addition to the core-correlation, core-polarization, and pair-correlation terms, significantly contributing terms such as $S_1^\dagger \overline{O} S_1$, $S_1^\dagger \overline{O} S_2 + S_2^\dagger \overline{O} S_1$, and $S_2^\dagger \overline{O} S_2$ are considered. Also, a large number of effective two-body terms, which are further contracted with the S and $S^\dagger$ operators, can contribute here [3]. Terms such as $S_{2v}^\dagger O T_1$ and $S_{2v}^\dagger O T_2$ are responsible for providing little correlations, but are accounted for in the present approach [3].

The mathematical expressions of the transition probabilities in s^{-1} corresponding to $E1$, $E2$, and $M1$ transitions for a channel of emission from k to i are represented by [40]

$$A_{ki}^{E1} = \frac{2.0261 \times 10^{18}}{\lambda^3 (2j_k + 1)} S_{ki}^{E1}, \tag{2.3}$$

$$A_{ki}^{E2} = \frac{1.1199 \times 10^{18}}{\lambda^5 (2j_k + 1)} S_{ki}^{E2}, \tag{2.4}$$

and

$$A_{ki}^{M1} = \frac{2.697 \times 10^{13}}{\lambda^3 (2j_k + 1)} S_{ki}^{M1}, \tag{2.5}$$

where λ (in angstroms) is the wavelength of the transition. Here $S_{ki}^{O} = (O_{ki})^2$ is the transition strength in a.u. The lifetime τ_k of a state k is calculated by considering all the channels of emission to the states i:

$$\tau_k = \sum_i \frac{1}{A_{ki}}. \tag{2.6}$$

The single-particle reduced matrix elements of the electric dipole $E1$, electric quadrupole $E2$, and magnetic dipole $M1$

transition operators and the operators associated with the magnetic dipole constant A and electric quadrupole hyperfine constant B are given in Ref. [41]. The hyperfine anomaly due to the Bohr-Weisskopf effect for any particular state is defined by [14,15]

$$\Delta\% = \frac{A_1 g_2 - A_2 g_1}{A_2 g_1} \times 100, \tag{2.7}$$

where A_1 and A_2 are the hyperfine constants and g_1 and g_2 are the corresponding g factors of the nuclei of the isotopes of concern.

III. RESULTS AND DISCUSSION

The DF orbitals are constructed here from the basis-set expansion technique [41,42]. The radial part of the basis is considered to have a Gaussian-type form. These Gaussian-type orbitals (GTOs) have two optimized parameters α_0 and β. For In III, these optimized parameters are expected to be 0.0073 and 2.65, respectively. To derive these estimations, we use the numerical values of bound orbital energies and the radial expectations of r and $1/r$ of these orbitals as obtained from the GRASP92 code [43]. In order to generate the DF orbitals, 32, 32, 30, 30, and 27 GTO bases are considered for the s, p, d, f, and g symmetries, respectively. The coupled-cluster calculations are performed with 12, 11, 10, 9, and 8 active orbitals for the above-mentioned symmetries. These of active orbitals include all the bound orbitals and the first few unbound orbitals. The number of symmetries and the number of active orbitals considered under each symmetry are consistent with the convergence criteria of core-correlation energy [3]. In the present work, the percentage of correlation contribution (the RCC result minus the DF result) to any property is defined with respect to the DF result.

In Table I we represent ionization potentials (IPs) of the ground state and few low-lying excited states in cm^{-1}. Our RCC results are compared with the experimental values obtained from the National Institute of Standards and Technology (NIST) [44]. The maximum difference between these values occurs in the case of the $4f\ ^2F_{5/2}$ state, which is about 0.44%.

In Table II we present the $E1$ transition amplitudes in length gauge form at the DF and RCC levels. The correlation contributions are presented in the same table. The wavelengths of these transitions, which are calculated from the IPs of the NIST, are listed in the second column of this table. The correlation effect decreases the transition amplitude in all cases except the transition $5s\ ^2S_{1/2} \rightarrow 6p\ ^2P_{1/2}$. We find that the correlation contribution is much larger than the DF values for the $5s\ ^2S_{1/2} \rightarrow 6p\ ^2P_{1/2,3/2}$ transitions, unlike the other cases [31]. These results have been observed also in velocity

TABLE I. Ionization potentials of ground and low-lying excited states in cm^{-1}.

State	RCC	NIST
$5s\,^2S_{1/2}$	226445.34	226191.3
$5p\,^2P_{1/2}$	168645.05	169010.2
$5p\,^2P_{3/2}$	164208.93	164668.1
$6s\,^2S_{1/2}$	99353.88	99317.1
$5d\,^2D_{3/2}$	97713.82	97738.5
$5d\,^2D_{5/2}$	97288.94	97448.8
$6p\,^2P_{1/2}$	81409.35	81607.7
$6p\,^2P_{3/2}$	80011.96	80268.7
$4f\,^2F_{5/2}$	63937.80	64222.5
$4f\,^2F_{7/2}$	63960.98	64214.5
$7s\,^2S_{1/2}$	56699.72	56761.5
$5g\,^2G_{7/2}$	39497.11	39669.3
$5g\,^2G_{9/2}$	39497.11	39669.3

gauge calculations. The two-resonance transitions $5s\,^2S_{1/2} \rightarrow 5p\,^2P_{1/2,3/2}$ are about -17.2% to -17.5% correlated and it has been estimated that most of their correlations come from the

core-polarization effect. The core polarization is also found to be the dominating mechanism in the transitions $5p\,^2P_{3/2} \rightarrow 5d\,^2D_{3/2,5/2}$ and $5p\,^2P_{1/2} \rightarrow 5d\,^2D_{3/2}$, where the total correlation contributions are about -11.8% to -12.2%. The oscillator strengths of $E1$ transitions calculated from the corresponding transition amplitudes and quoted wavelengths are also presented in Table II. These transitions are astrophysically important [20] and fall in the visible and ultraviolet regions of the electromagnetic spectrum.

Table II also shows the discrepancies among various theoretical and experimental results. Our highly correlated *ab initio* calculations show excellent agreement with the model potential [45] and relativistic many-body perturbation theory (RMBPT) calculations [28]. Here the experimental results are evaluated using the corresponding lifetime measurements [27,46] and the NIST wavelengths [44]. Considerable differences are noted between the experimentally measured values and all the theoretical results for the $5p\,^2P_{1/2} \rightarrow 5d\,^2D_{3/2}$ and $5p\,^2P_{3/2} \rightarrow 6s\,^2S_{1/2}$ transitions. Therefore, more precise experiments may be desirable for these cases. Our calculated RCC results are consistent with Cowan's prediction of the oscillator strength ratio in the

TABLE II. Calculated $E1$ transition amplitudes (in a.u.) and oscillator strengths. The corresponding wavelengths λ are presented in angstroms. Here Corr. denotes the correlation contributions. The oscillator strengths calculated by other theories (Theor.) and experimental measurements (Expt.) are also reported for comparison with our relativistic coupled-cluster results.

Transitions	λ	Transition amplitudes			Oscillator strengths		
		DF	Corr.	RCC	RCC	Theor.	Expt.
$5s\,^2S_{1/2} \rightarrow 5p\,^2P_{1/2}$	1748.83	2.0868	-0.3656	1.7212	0.2600	0.2519,[a] 0.260[b] 0.260,[e] 0.1963[f] 0.2486[a]	0.27,[c] 0.2796[d]
$\rightarrow 5p\,^2P_{3/2}$	1625.40	2.9512	-0.5070	2.4442	0.5647	0.5478,[a] 0.567[b] 0.278,[e] 0.4248[f] 0.5400[a]	0.60,[c] 0.5279[d]
$\rightarrow 6p\,^2P_{1/2}$	691.64	0.0324	0.1130	0.1454	0.0047	0.0003[f]	
$\rightarrow 6p\,^2P_{3/2}$	685.30	0.0403	-0.1653	-0.1250	0.0035	0.0007[f]	
$5p\,^2P_{1/2} \rightarrow 6s\,^2S_{1/2}$	1434.86	1.2795	-0.0473	1.2322	0.1598	0.161[b]	
$\rightarrow 5d\,^2D_{3/2}$	1403.08	3.3519	-0.4100	2.9419	0.9323	0.9113,[a] 0.900[b]	0.7870[d]
$\rightarrow 7s\,^2S_{1/2}$	890.88	0.3917	-0.0031	0.3886	0.0257		
$5p\,^2P_{3/2} \rightarrow 6s\,^2S_{1/2}$	1530.20	1.9776	-0.0774	1.9002	0.1778	0.179[b]	0.2506[d]
$\rightarrow 5d\,^2D_{3/2}$	1494.11	1.5574	-0.1837	1.3737	0.0954	0.0932,[a] 0.092[b]	
$\rightarrow 5d\,^2D_{5/2}$	1487.67	4.6559	-0.5481	4.1078	0.8575	0.8387,[a] 0.831[b]	0.8585[d]
$\rightarrow 7s\,^2S_{1/2}$	926.73	0.5786	-0.0095	0.5691	0.0265		
$6s\,^2S_{1/2} \rightarrow 6p\,^2P_{1/2}$	5646.72	4.3068	-0.2107	4.0961	0.4573	0.3708[f]	
$\rightarrow 6p\,^2P_{3/2}$	5249.79	6.0411	-0.2907	5.7504	0.9714	0.7884[f]	
$5d\,^2D_{3/2} \rightarrow 6p\,^2P_{1/2}$	6199.32	4.1135	-0.1120	4.0015	0.1983		
$\rightarrow 6p\,^2P_{3/2}$	5724.16	1.7862	-0.0453	1.7409	0.0407		
$\rightarrow 4f\,^2F_{5/2}$	2983.65	7.0372	-0.4556	6.5816	1.1110	1.0915[a]	1.1771[d]
$5d\,^2D_{5/2} \rightarrow 6p\,^2P_{3/2}$	5820.69	5.4252	-0.1366	5.2885	0.2446		
$\rightarrow 4f\,^2F_{5/2}$	3009.66	1.8915	-0.1213	1.7702	0.0529	0.0520[a]	
$\rightarrow 4f\,^2F_{7/2}$	3008.94	8.4595	-0.5422	7.9173	1.0711	1.0394[a]	1.0522[d]
$6p\,^2P_{1/2} \rightarrow 7s\,^2S_{1/2}$	4024.76	2.7944	-0.0806	2.7138	0.2764		
$6p\,^2P_{3/2} \rightarrow 7s\,^2S_{1/2}$	4254.02	4.2633	-0.1228	4.1405	0.3035		

[a]Third-order relativistic many-body perturbation theory [28,52].
[b]Core-polarized augmented Dirac-Fock method [45].
[c]Beam foil technique [27].
[d]Beam foil technique [46].
[e]Configuration-interaction calculation [29].
[f]Relativistic quantum-defect orbital method [31].

TABLE III. Calculated $E2$ and $M1$ transition amplitudes in a.u. The corresponding wavelengths λ are presented in angstroms. Here Corr. denotes the correlation contributions.

Transitions	λ	$E2$			$M1$		
		DF	Corr.	RCC	DF	Corr.	RCC
$5s\,^2S_{1/2} \rightarrow 5d\,^2D_{3/2}$	778.50	6.8096	-0.6241	6.1855			
$\rightarrow 5d\,^2D_{5/2}$	776.74	8.3060	-0.7744	7.5316			
$5p\,^2P_{1/2} \rightarrow 5p\,^2P_{3/2}$	23030.33	8.7362	-0.7523	7.9839	1.1532	0.0001	1.1533
$\rightarrow 6p\,^2P_{3/2}$	1126.87	5.1577	-0.4127	4.7450	0.0317	0.0011	0.0328
$\rightarrow 4f\,^2F_{5/2}$	954.31	11.5617	-1.0246	10.5371			
$5p\,^2P_{3/2} \rightarrow 6p\,^2P_{1/2}$	1203.94	6.1114	-0.4543	5.6571	0.0336	0.0008	0.0344
$\rightarrow 6p\,^2P_{3/2}$	1184.84	5.7550	-0.4327	5.3223	0.0003	0.0006	0.0009
$\rightarrow 4f\,^2F_{5/2}$	995.56	6.5714	-0.5601	6.0113			
$\rightarrow 4f\,^2F_{7/2}$	995.48	16.1049	-1.3733	14.7316			
$6s\,^2S_{1/2} \rightarrow 5d\,^2D_{3/2}$	63347.27	20.8068	-1.1669	19.6399			
$\rightarrow 5d\,^2D_{5/2}$	53524.59	25.7109	-1.4279	24.2830			
$5d\,^2D_{3/2} \rightarrow 5d\,^2D_{5/2}$	345184.67	12.5903	-0.8226	11.7677	1.5491	0.0001	1.5492
$\rightarrow 7s\,^2S_{1/2}$	2440.39	6.9372	-0.3581	6.5791			
$5d\,^2D_{5/2} \rightarrow 7s\,^2S_{1/2}$	2457.77	8.7467	-0.4355	8.3112			
$6p\,^2P_{1/2} \rightarrow 6p\,^2P_{3/2}$	74682.60	37.2585	-2.0824	35.1762	1.1531	0.0000	1.1531
$\rightarrow 4f\,^2F_{5/2}$	5752.02	40.9209	-2.2989	38.6220			
$6p\,^2P_{3/2} \rightarrow 4f\,^2F_{5/2}$	6232.01	22.1480	-1.2351	20.9129			
$\rightarrow 4f\,^2F_{7/2}$	6228.90	54.1958	-3.0186	51.1772			
$4f\,^2F_{5/2} \rightarrow 4f\,^2F_{7/2}$	12500000	17.8540	-1.0507	16.8033	1.8516	0.0001	1.8517

$5D$-$5P$ multiplet [47]. The experimental value agrees well with the RCC value for the transition $5p\,^2P_{3/2} \rightarrow 5d\,^2D_{5/2}$. Therefore, the experimental result of the $5p\,^2P_{1/2} \rightarrow 5d\,^2D_{3/2}$ transition does not follow Cowan's prediction. A recent experiment [23] claims accurate estimations of absorption coefficients of 298.28-, 300.808-, and 524.877-nm transition lines, where our calculated amplitudes can be used.

Though electromagnetically forbidden transitions do not contribute significantly to the lifetimes of the excited states

here, they are important in different areas of physics [41,48]. The magnetic dipole ($M1$) transition rate between the fine-structure states of $4f\,^2F$ has been calculated using the multiconfiguration Dirac-Fock (MCDF) method [32]. Our calculated fine-structure splitting (-23 cm^{-1}) of this term is much closer to the central experimental value (8 cm^{-1}) [44] compared to the MCDF calculation (-71 cm^{-1}). The latter calculation estimated a comparatively large correlation contribution as the DF value is -24 cm^{-1}. There is a discrepancy between the MCDF and our calculations of transition amplitude between these fine-structure states, where the

FIG. 1. Comparison between $E2$ and $M1$ transition probabilities (s^{-1}) on a log$_{10}$ scale. The transitions between levels are presented along the x axis and the transition probabilities are presented along the y axis. The levels are identified as follows: 1, $5s\,^2S_{1/2}$; 2, $5p\,^2P_{1/2}$; 3, $5p\,^2P_{3/2}$; 4, $6s\,^2S_{1/2}$; 5, $5d\,^2D_{3/2}$; 6, $5d\,^2D_{5/2}$; 7, $6p\,^2P_{1/2}$; 8, $6p\,^2P_{3/2}$; and 9, $7s\,^2S_{1/2}$.

TABLE IV. Calculated lifetimes using the relativistic coupled-cluster theory of some low-lying states in 10^{-9} s along with their comparisons with the other theoretical (Theor.) and experimental (Expt.) results.

State	RCC	RMBPT[a]	Theor.[b]	Expt.
$5p\,^2P_{1/2}$	1.78	1.84	1.26	1.45 ± 0.10,[c] 1.72 ± 0.07[d]
$5p\,^2P_{3/2}$	1.42	1.45		1.50 ± 0.15[d]
$6s\,^2S_{1/2}$	0.65			
$5d\,^2D_{3/2}$	0.53	0.67	0.56	0.75 ± 0.06[d]
$5d\,^2D_{5/2}$	0.58	0.61		0.98 ± 0.10,[c] 0.58 ± 0.05[d]
$6p\,^2P_{1/2}$	4.40			
$6p\,^2P_{3/2}$	4.54			
$4f\,^2F_{5/2}$	1.70	1.82		1.70 ± 0.07[d]
$4f\,^2F_{7/2}$	1.72	1.74		1.72 ± 0.07[d]
$7s\,^2S_{1/2}$	1.03			
$5g\,^2G_{7/2}$	2.65			
$5g\,^2G_{9/2}$	2.66	2.71		2.84 ± 0.30[d]

[a]Reference [28].
[b]Relativistic Hartree-Fock theory [30].
[c]Beam foil technique [27].
[d]Beam foil technique [46].

TABLE V. Calculated hyperfine constant A along with the different correlation contributing terms in MHz. Here Norm. denotes the normalization correction.

State	d	$\bar{d}$	$\bar{d}S_1$	$\bar{d}S_2$	$S_1^\dagger \bar{d} S_1$	$S_1^\dagger \bar{d} S_2$	$S_2^\dagger \bar{d} S_2$	Norm.	RCC
$5s\ ^2S_{1/2}$	17672.45	17635.18	2392.83	1382.51	81.21	72.73	345.29	-395.71	21358.30
$5p\ ^2P_{1/2}$	3317.77	3315.07	576.20	218.52	25.13	17.50	48.24	-66.76	4107.07
$5p\ ^2P_{3/2}$	514.01	518.29	89.92	68.51	3.92	5.10	22.45	-10.91	693.70
$6s\ ^2S_{1/2}$	4792.83	4779.14	318.36	340.26	5.32	2.40	106.62	-47.66	5467.19
$5d\ ^2D_{3/2}$	97.59	100.98	19.73	22.30	0.99	1.40	5.26	-1.16	149.53
$5d\ ^2D_{5/2}$	41.01	42.38	8.24	11.11	0.41	0.66	0.33	-0.49	62.63
$6p\ ^2P_{1/2}$	1090.79	1089.88	97.20	76.63	2.22	2.27	12.99	-11.97	1262.70
$6p\ ^2P_{3/2}$	173.61	174.80	16.01	23.18	0.38	0.53	11.54	-2.11	223.49
$4f\ ^2F_{5/2}$	2.60	2.65	0.48	-2.52	0.03	-0.24	1.73	-0.01	2.14
$4f\ ^2F_{7/2}$	1.45	1.49	0.27	-3.32	0.02	-0.41	0.03	0.01	-1.91
$7s\ ^2S_{1/2}$	2234.71	2227.97	-0.49	153.23	0.01	-4.34	53.48	-16.63	2396.80

former is evaluated from their calculated transition probability and wavelength. The discrepancy probably can be avoided with the proper choice of initial and final states and use of the NIST wavelength [44].

The $E2$ and $M1$ transition amplitudes along with their corresponding NIST wavelengths (λ values), are presented in Table III. The correlation contributions to all the $E2$ transitions reduce the corresponding DF values and vary from -4.9% to -9.3%. The $5s\ ^2S_{1/2} \rightarrow 5d\ ^2D_{3/2,5/2}$ transitions are maximally correlated by -9.2% to -9.3% with respect to all others $E2$ transitions presented here. It has been observed (see Fig. 1) that $M1$ transition probabilities are stronger than $E2$ probabilities for transitions among fine-structure states.

In Table IV we compare our calculated lifetimes for some low-lying states with other theoretically calculated and experimentally measured values. The experimental wavelengths from the NIST are used in our calculations. The beam foil experiment of Andersen *et al.* [27] and the relativistic Hartree-Fock calculation [30] of Cheng and Kim underestimate the lifetime of the $5p\ ^2P_{1/2}$ state. Our estimated lifetimes are in good agreement with the measured values of Ansbacher *et al.* [46] and calculated results obtained using the RMBPT method [28], except in the case of the $5d\ ^2D_{3/2}$ state. The lifetime of the

$5d\ ^2D_{3/2}$ state measured by the beam foil experiment [46] and calculated by the RMBPT method are 0.75 ± 0.06 and 0.67 ns, respectively. These lifetimes are based only on the transition $5d\ ^2D_{3/2} \rightarrow 5p\ ^2P_{1/2}$. In contrast, considering both channels of emission $5d\ ^2D_{3/2} \rightarrow 5p\ ^2P_{1/2}$ and $5d\ ^2D_{3/2} \rightarrow 5p\ ^2P_{3/2}$, our RCC calculations yield this lifetime as 0.53×10^{-9} s. Nevertheless, considering the individual channel, we find the lifetimes of $5d\ ^2D_{3/2} \rightarrow 5p\ ^2P_{1/2}$ and $5d\ ^2D_{3/2} \rightarrow 5p\ ^2P_{3/2}$ transitions to be 0.63 and 3.49 ns, respectively. Similar arguments hold also in a comparison of the lifetimes of the $4f\ ^2F_{5/2}$ state, where our calculations considered all the channels of emissions compared to other results that account for emission through only the dominating channel. However, for the $5d\ ^2D_{5/2}$ state there is only one dominating channel $5d\ ^2D_{5/2} \rightarrow 5p\ ^2P_{3/2}$; therefore, we find good agreement with experiment [46] here. Anderson *et al.* also overestimate the lifetime of this state. The corrections due to the $E2$ and/or $M1$ transitions in the calculations of all the lifetime values are at or beyond the fourth decimal place in the unit of nanoseconds. This may be important for ultrafast spectroscopy [49].

The accurate estimation of the large hyperfine splitting of the ground state of ^{115}In III is one of the most important objectives of this work. The magnetic dipole and the electric
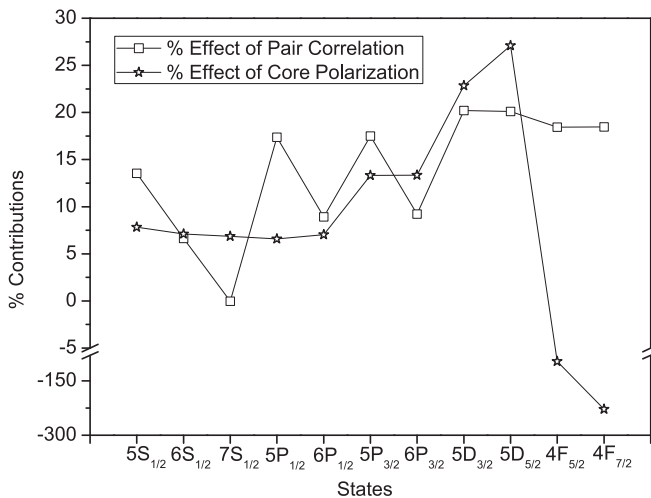
FIG. 2. Percentage of the core-polarization and pair-correlation contributions to the constant A.
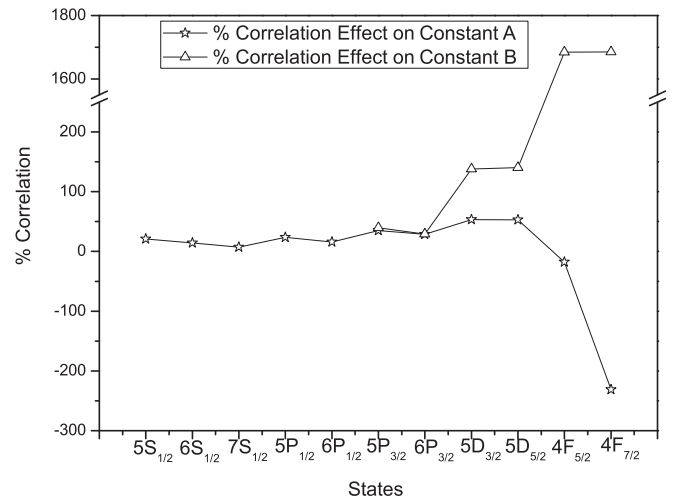
FIG. 3. Percentage of correlation to the hyperfine constants A and B.

TABLE VI. Calculated hyperfine constant B along with the different correlation contributing terms in MHz. Here Norm. denotes the normalization correction.

State	d	$\bar{d}$	$\bar{d}S_1$	$\bar{d}S_2$	$S_1^\dagger \bar{d} S_1$	$S_1^\dagger \bar{d} S_2$	$S_2^\dagger \bar{d} S_2$	Norm.	RCC
$5p\,^2P_{3/2}$	648.57	651.06	113.13	138.88	4.94	6.17	10.05	−14.25	905.47
$5d\,^2D_{3/2}$	41.02	42.56	8.32	45.33	0.42	1.76	−0.06	−0.76	97.57
$5d\,^2D_{5/2}$	55.79	57.76	11.22	63.38	0.56	2.43	−0.30	−1.04	134.00
$6p\,^2P_{3/2}$	219.07	219.75	20.19	41.75	0.47	0.37	3.51	−2.66	282.32
$4f\,^2F_{5/2}$	1.76	1.86	0.34	28.28	0.03	1.30	−0.30	−0.15	31.36
$4f\,^2F_{7/2}$	2.06	2.17	0.40	33.15	0.03	1.53	−0.31	−0.18	36.79
$5g\,^2G_{7/2}$	0.31	0.31	0.00	7.08	0.00	0.04	−0.05	0.00	7.39
$5g\,^2G_{9/2}$	0.33	0.33	0.00	7.73	0.00	0.05	−0.05	0.00	8.06

quadrupole moments of the stable ^{115}In isotope are considered to be 5.5408(2) nuclear magnetons and 0.810 b, respectively, from Ref. [9], with nuclear spin parity $9/2^+$. In Table V the hyperfine constant A of the ground and a few excited states is presented at the DF and RCC levels along with the contributions of different correlation terms. The term d is the Dirac-Fock contribution, $\bar{d}$ is the contribution from the Dirac-Fock and core-correlation contribution, and $\bar{d}S_1$ and $\bar{d}S_2$ represent the pair-correlation and core-polarization contributions, respectively, including the conjugate terms. The other terms $S_1^\dagger \bar{d} S_1$, $S_1^\dagger \bar{d} S_2$, and $S_2^\dagger \bar{d} S_2$ also considered the conjugate terms. Here Norm. represents the normalization correction. Such a term-by-term analysis was presented earlier in the constant-A calculations of ^{113}Cd$^+$, where the correlation exhaustiveness of the present method was well established [3]. The largest correlation contributions come from the pair-correlation terms for the $5s\,^2S_{1/2}$, $5p\,^2P_{1/2,3/2}$, and $6p\,^2P_{1/2}$ states, whereas the core polarization contributes the most to the $6s\,^2S_{1/2}$, $7s\,^2S_{1/2}$, $5d\,^2D_{3/2,5/2}$, $6p\,^2P_{3/2}$, and $4f\,^2F_{5/2,7/2}$ states. These are graphically presented in Fig. 2. It is also clear from Fig. 2 that the pair-correlation contributions to the outer orbitals are decreasing along the same relativistic symmetry, which is expected [50]. The percentage of pair-correlation contribution being almost identical for the fine-structure states of any term has also been observed [42]. The $4f\,^2F_{5/2}$ and

$4f\,^2F_{7/2}$ states show a large percentage of negative core-polarization contributions. These large negative contributions dominantly arise from the exchange part of these correlation terms. The constant A of the low-lying bound state $ns\,^2S_{1/2}$ falls in the GHz range and its high value is expected to be due to the large overlap of its wave functions in the nuclear vicinity. The total correlation contribution to the constant A of the ground state is around 20.9 %. The estimated hyperfine constant A of all these states is presented within an approximate theoretical uncertainty of around $\pm 2\%$.

Our calculated hyperfine constant B for the low-lying states is presented in Table VI along with the different correlation-contributing many-body terms. In this table the labeling of the different terms is the same as in Table V. The percentages of the total correlation contributions to the constants A and B are plotted in Fig. 3 to get an idea of their relative responses. The correlation to the $4f\,^2F$ states shows an opposite trend between these two constants. This may be a consequence of the difference in the behavior of the wave functions in two different radial regions of nuclear proximity. Here one can see that the core polarization contributes strongly to all the cases with respect to the other correlation terms. This is clear from Table VI and Fig. 4. Even the RCC values of the $5d\,^2D_{3/2,5/2}$ states become more than twice their corresponding DF values due to large core-polarization effects. The correlation contributions to the hyperfine constant B of the $4f\,^2F_{5/2,7/2}$ and $5g\,^2G_{7/2,9/2}$
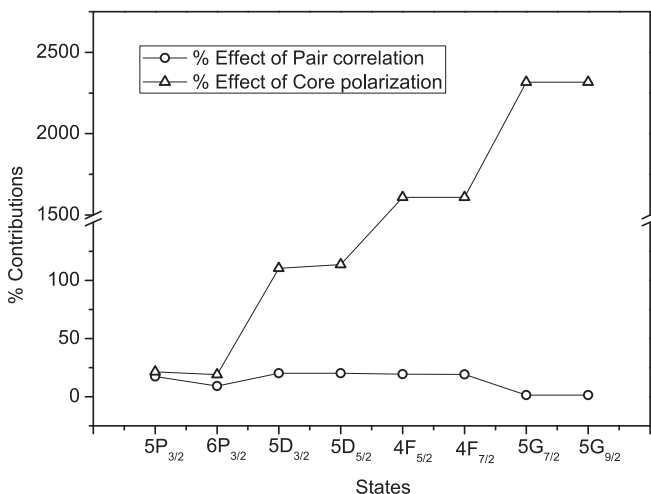
FIG. 4. Percentage of the core-polarization and pair-correlation contributions to the constant B.

TABLE VII. Hyperfine splitting of the ground and a few low-lying excited states in MHz. The percentage contributions from the constant B to these splitting are presented in the last column.

State	$F_1 \leftrightarrow F_2$	Splitting	B
$5s\,^2S_{1/2}$	$5 \leftrightarrow 4$	106791.51	0
$5p\,^2P_{1/2}$	$5 \leftrightarrow 4$	20535.37	0
$5p\,^2P_{3/2}$	$6 \leftrightarrow 5$	4765.84	12.67
	$5 \leftrightarrow 4$	3279.86	−5.75
$6s\,^2S_{1/2}$	$5 \leftrightarrow 4$	27335.95	0
$5d\,^2D_{3/2}$	$6 \leftrightarrow 5$	962.22	6.76
	$5 \leftrightarrow 4$	727.31	−2.79
$5d\,^2D_{5/2}$	$7 \leftrightarrow 6$	500.92	12.48
	$6 \leftrightarrow 5$	385.81	2.61
$6p\,^2P_{1/2}$	$5 \leftrightarrow 4$	6313.48	0
$6p\,^2P_{3/2}$	$6 \leftrightarrow 5$	1529.17	12.31
	$5 \leftrightarrow 4$	1058.64	−5.56
$7s\,^2S_{1/2}$	$5 \leftrightarrow 4$	11984.02	0

TABLE VIII. Hyperfine anomaly of In III.

State	A (113)	A (115)	A (117)	$^{113}\Delta^{115}$ (%)	$^{115}\Delta^{117}$ (%)
$5s\ ^2S_{1/2}$	21313.0636	21358.3017	21271.3821	0.007491126	0.009042670
$6s\ ^2S_{1/2}$	5455.6089	5467.1903	5444.9430	0.007461625	0.009008028
$7s\ ^2S_{1/2}$	2391.7256	2396.8034	2387.0509	0.007438228	0.008981253
$5p\ ^2P_{1/2}$	4098.0919	4107.0750	4090.7031	0.000558990	0.000676622
$5p\ ^2P_{3/2}$	692.1824	693.6997	690.9345	0.000553917	0.000670590
$6p\ ^2P_{1/2}$	1259.9349	1262.6970	1257.6639	0.000534891	0.000641958
$6p\ ^2P_{3/2}$	223.0038	223.4925	222.6013	0.000642552	0.000779395

states change abnormally from the DF to the RCC levels. These abnormal changes are also guided by the core-polarization effects. One can also find in Fig. 4 that the percentage of contribution of the core polarization is almost the same for the fine-structure states of a term.

The hyperfine splitting of the ground as well as a few low-lying excited states is presented in Table VII. The percentage of contributions from the constant B to the splitting values is presented in the last column of this table. The comparison of theoretically estimated [7] and experimentally measured [4] hyperfine constants of different states shows that the nuclear magnetic moment may be $5.4422\mu_B$ for ^{115}In I. This value varies from the standard value, obtained from Raghavan, of $5.5408\mu_B$ [9]. This changes the ground-state splitting by 0.0634 cm^{-1}, which is substantial in terms of the accuracy we are looking for.

Study of the nuclear magnetization distribution of any atomic system provides information about nuclear wave functions, which is very important for the PNC calculations [18]. It is difficult to measure the nuclear magnetization distribution experimentally [18,51]; rather it can be estimated from an accurate value of the hyperfine splitting using the Bohr-Weisskoff formalism [14]. Though the mean contribution of this effect appears only for $S_{1/2}$ and $P_{1/2}$ states, other states, such as $P_{3/2}$, are effected due to the e^--e^- interaction. Using Eq. (2.3), we have calculated the hyperfine anomaly of In III isotopes between 113 and 115 ($^{113}\Delta^{115}$%) and 115 and 117 ($^{115}\Delta^{117}$%). We present these results in Table VIII. Like neutral

indium, we observe a considerable effect of the finite nucleus on these parameters for In III [15]. However, we do not see significant changes in the parameter between $P_{1/2}$ and $P_{3/2}$ states as was observed in the neutral system [14,15].

IV. CONCLUSION

The electromagnetic transition amplitudes, lifetimes, and hyperfine constants are calculated using a highly correlated theoretical approach with a proper account of relativity. Our calculated transition line parameters can be applied for abundance estimations in different astronomical systems and laboratory plasmas. The ground-state hyperfine splitting of this ion predicts its use as a microwave frequency standard at 10^{-11} s. A detailed analysis of the different correlation-contributing terms associated with the coupled-cluster theory show their impact on the calculations of the hyperfine constants. The hyperfine constant B of the fine structures of the $4f\ ^2F$ and $5g\ ^2G$ terms is found to be abnormally correlated due to the very strong influence of the core polarization. The calculated hyperfine splitting can be used for accurate line-profile analysis of astrophysically important transition lines. We have also observed distinct features in the hyperfine anomaly parameters compared to neutral indium.

[1] M. M. Schauer, J. R. Danielson, D. Feldbaum, M. S. Rahaman, L. B. Wang, J. Zhang, X. Zhao, and J. R. Torgerson, Phys. Rev. A **82**, 062518 (2010).

[2] B. M. Jelenkovic, S. Chung, J. D. Prestage, and L. Maleki, Phys. Rev. A **74**, 022505 (2006).

[3] G. Dixit, H. S. Nataraj, B. K. Sahoo, R. K. Chaudhuri, and S. Majumder, Phys. Rev. A **77**, 012718 (2008).

[4] M. Gunawardena, H. Cao, P. W. Hess, and P. K. Majumder, Phys. Rev. A **80**, 032519 (2009).

[5] T. G. Eck, A. Lurio, and P. Kusch, Phys. Rev. **106**, 954 (1957).

[6] A. K. Mann and P. Kusch, Phys. Rev. **77**, 427 (1950).

[7] M. Das, R. K. Chaudhuri, S. Chattopadhyay, and U. S. Mahapatra, J. Phys. B **44**, 065003 (2011).

[8] U. I. Safronova, M. S. Safronova, and M. G. Kozlov, Phys. Rev. A **76**, 022501 (2007).

[9] P. Raghaavn, At. Data Nucl. Data Tables **42**, 189 (1989).

[10] E. N. Fortson, Y. Pang, and L. Wilets, Phys. Rev. Lett. **65**, 2857 (1990).

[11] A. Marie and M. Pendrill, Hyperfine Interact. **127**, 41 (2000).

[12] J. R. Crespo López-Urrutia, P. Beiersdorfer, K. Widmann, B. B. Birkett, A.-M. Mårtensson-Pendrill, and M. G. H. Gustavsson, Phys. Rev. A **57**, 879 (1998).

[13] S. H. Devare, H. G. Devare, F. Pleiter, F. C. Magendans, and L. Niesen, Hyperfine Interact. **15/16**, 31 (1983).

[14] J R Persson, At. Data Nucl. Data Tables **99**, 62 (2013).

[15] O. Lutz, A. Nolle, and A. Uhl, Z. Phys. **248**, 159 (1971).

[16] A. Bohr and V. F. Weisskopf, Phys. Rev. **77**, 94 (1950).

[17] S. Buettgenbach, Hyperfine Interact. **20**, 1 (1984).

[18] H. H. Stroke, H. T. Duong, and J. Pinard, Hyperfine Interact. **129**, 319 (2000).

[19] S. Djeniže, A. Srećković, and S. Bukvić, Spectrochim. Acta B **61**, 588 (2006).

[20] Z. Simic, M. S. Dimitrijevic, A. B. Kovacevic, and S. Sahal-Brechot, Baltic Astron. **20**, 613 (2011), arXiv:1201.2023.

[21] C. R. Cowley, M. R. Hartoog, and A. P. Cowley, Astrophys. J. **194**, 343 (1974).

[22] N. Vitas, I. Vince, M. Lugaro, O. Andriyenko, M. Gošić, and R. J. Rutten, Mon. Not. R. Astron. Soc. **384**, 370 (2008).

[23] M. Skočić, M. Burger, S. Bukvić, and S. Djeniže, J. Phys. B **45**, 225701 (2012).

[24] M. A. Ali and Y.-K. Kim, Phys. Rev. A **38**, 3992 (1988).

[25] R. A. Nodwell, Ph.D. thesis, University of British Columbia, 1956.

[26] K. S. Bhatia, J. Phys. B **11**, 2421 (1978).

[27] T. Andersen, A. Kirkegard Nielsen, and G. Sorensen, Phys. Scr. **6**, 122 (1972).

[28] U. I. Safronova, I. M. Savukov, M. S. Safronova, and W. R. Johnson, Phys. Rev. A **68**, 062505 (2003).

[29] L. Glowacki and J. Migdalek, Phys. Rev. A **80**, 042505 (2009).

[30] K.-t. Cheng and Y.-K. Kim, J. Opt. Soc. Am. **69**, 125 (1979).

[31] I. Martin, M. A. Almaraz, and C. Lavin, Z. Phys. D **35**, 239 (1995).

[32] X.-B. Ding, F. Koike, I. Murakami, D. Kato, H. A. Sakaue, C.-Z. Dong, and N. Nakamura, J. Phys. B **45**, 035003 (2012).

[33] N. N. Dutta and S. Majumder, Phys. Rev. A **85**, 032512 (2012).

[34] N. N. Dutta and S. Majumder, Astrophys. J. **737**, 25 (2011).

[35] R. F. Bishop and H. G. Kummel, Phys. Today **40**(3), 52 (1987).

[36] I. Lindgren and D. Mukherjee, Phys. Rep **151**, 93 (1987).

[37] A. Szabo and N. S. Ostlund, *Modern Quantum Chemistry: Introduction to Advanced Electronic Structure Theory* (Dover, Mineola, 1996).

[38] G. Gopakumar, H. Merlitz, S. Majumder, R. K. Chaudhuri, B. P. Das, U. S. Mahapatra, and D. Mukherjee, Phys. Rev. A **64**, 032502 (2001).

[39] B. K. Mani and D. Angom, Phys. Rev. A **81**, 042514 (2010).

[40] G. Dixit, H. S. Nataraj, B. K. Sahoo, R. K. Chaudhuri, and S. Majumder, J. Phys. B **41**, 025001 (2008).

[41] N. N. Dutta, S. Roy, G. Dixit, and S. Majumder, Phys Rev. A **87**, 012501 (2013).

[42] N. N. Dutta and S. Majumder, Phys. Rev. A **88**, 062507 (2013).

[43] F. A. Parpia, C. F. Fischer, and I. P. Grant, Comput. Phys. Commun. **175**, 745 (2006).

[44] NIST Atomic Spectra Database, version 5.0 (National Institute of Standards and Technology, Gaithersburg, 2012), http://physics.nist.gov/asd.

[45] J. Migdalek and M. Garmulewicz, J. Phys. B **33**, 1735 (2000).

[46] W. Ansbacher, E. H. Pinnington, J. A. Kernahan, and R. N. Gosselin, Can. J. Phys. **64**, 1365 (1986).

[47] R. D. Cowan, *The Theory of Atomic Structure and Spectra* (University of California Press, Berkeley, 1981).

[48] G. Dixit, B. K. Sahoo, R. K. Chaudhuri, and S. Majumder, Phys. Rev. A **76**, 042505 (2007).

[49] P. Sancho, arXiv:1311.0998.

[50] A. Owusu, R. W. Dougherty, G. Gowri, T. P. Das, and J. Andriessen, Phys. Rev. A **56**, 305 (1997).

[51] S. Buttgenbach, Hyperfine Interact. **20**, 1 (1984).

[52] H. S. Chou and W. R. Johnson, Phys. Rev. A **56**, 2424 (1997).